Eur Phys J C **33**, s01, s5–s20 (2004)
Digital Object Identifier (DOI) 10.1140/epjcd/s2004-03-1692-8

EPJ C direct
electronic only

Experimental tests of the standard model

P.S. Wells

CERN, CH-1211 Geneva 23, Switzerland

Received: 19 January 2004 / Accepted: 20 January 2004 /
Published Online: 24 February 2004 – © Springer-Verlag / Società Italiana di Fisica 2004

Abstract. Tests of the electroweak sector of the Standard Model are reviewed. The majority of new results come from LEP and the Tevatron. There are also developments in experimental input to the theoretical prediction of the muon $(g-2)$. The Standard Model successfully describes diverse measurements over a range of energy scales. The largest discrepancies are only at the three standard deviation level, with no strong hint for physics beyond the Standard Model.

PACS. 12.15.-y Electroweak interactions – 13.40.Em Electric and magnetic moments – 13.66.Fg Gauge and Higgs bosons in e^+e^- – 13.66.Jn Precision measurements in e^+e^- – 13.85.-t Hadron induced high-E interactions – 14.65.Ha Top quarks – 14.70.Fm W bosons – 14.70.Hp Z bosons – 14.80.Bn SM Higgs

1 Introduction

This review covers tests of the electroweak sector of the Standard Model. Other aspects of the Standard Model are covered by other speakers, including QCD, heavy flavour physics, the CKM matrix and CP violation. The emphasis is on results that have been updated since last summer [1]. Most of the recent results come from the LEP e^+e^- and the Tevatron $p\bar{p}$ colliders. The last relevant results from LEP1 at the Z pole are now being finalised, specifically heavy flavour forward-backward asymmetries. Measurements of gauge boson production and decay are also being finalised from LEP2, and the first results from the Tevatron Run II on gauge bosons and top physics are available. There are also updates to the status of the muon $(g-2)$ measurement, where the interplay of theory and experimental inputs is particularly important. The last part of the review covers global electroweak fits and implications for the Higgs boson mass.

2 LEP and SLD at the Z pole

The LEP collider delivered a total integrated luminosity of 1000 pb^{-1} between 1989 and 2000. The experiments ALEPH, DELPHI, L3 and OPAL recorded 4.5 million Z decays per experiment, including off-peak data. The SLD experiment at SLC recorded about 600 thousand Z decays with the important difference that the e^- beam was up to 77% polarised.

Measurements from LEP of the Z lineshape, lepton-pair forward-backward and τ polarisation asymmetries, and from SLD of the left-right asymmetry and double A^{ℓ}_{LRFB} asymmetries, have been final for some time. However, new heavy flavour forward-backward asymmetry results have been released by DELPHI and OPAL [2].

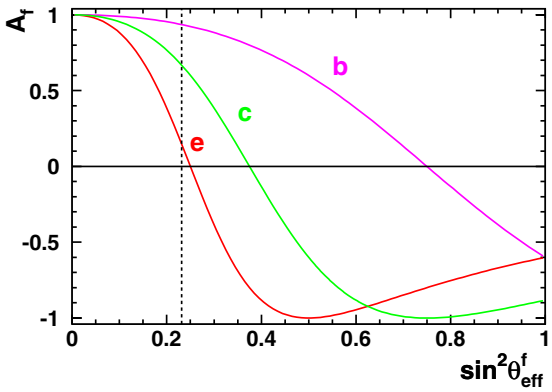

Fig. 1. Variation of $\mathcal{A}_{\mathrm{f}}$ with $\sin^2\theta^{\mathrm{lept}}_{\mathrm{eff}}$

The forward-backward asymmetry at LEP is given by

$$A_{\mathrm{FB}} = \frac{\sigma_{\mathrm{F}} - \sigma_{\mathrm{B}}}{\sigma_{\mathrm{F}} + \sigma_{\mathrm{B}}} ,$$

where σ_{F} is the cross-section for producing events where the angle θ between the incoming electron and outgoing fermion momentum vectors satisfies $\theta < 90°$.

The Z couplings to fermions are given by

$$g_{\mathrm{Vf}} = \sqrt{\rho}\left(T^3_{\mathrm{f}} - 2Q_{\mathrm{f}}\sin^2\theta^{\mathrm{f}}_{\mathrm{eff}}\right) ; \; g_{\mathrm{Af}} = \sqrt{\rho}\, T^3_{\mathrm{f}} .$$

The Z partial widths are related to $g^2_{\mathrm{Vf}} + g^2_{\mathrm{Af}}$, and the asymmetries to the ratio $g_{\mathrm{Vf}}/g_{\mathrm{Af}} = 1 - 4|Q_{\mathrm{f}}|\sin^2\theta^{\mathrm{f}}_{\mathrm{eff}}$. Coupling parameters $\mathcal{A}_{\mathrm{f}}$ are defined by

$$\mathcal{A}_{\mathrm{f}} = 2\frac{g_{V\mathrm{f}}\, g_{A\mathrm{f}}}{g^2_{V\mathrm{f}} + g^2_{A\mathrm{f}}} .$$

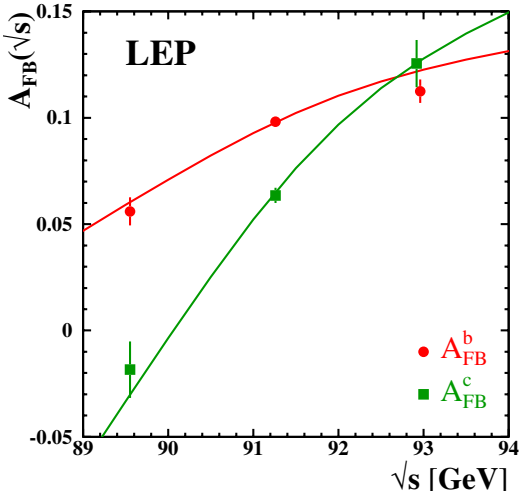

Fig. 2. Measurements of $A_{\rm FB}^{\rm b\bar{b}}$ and $A_{\rm FB}^{\rm c\bar{c}}$ as a function of $\sqrt{s}$

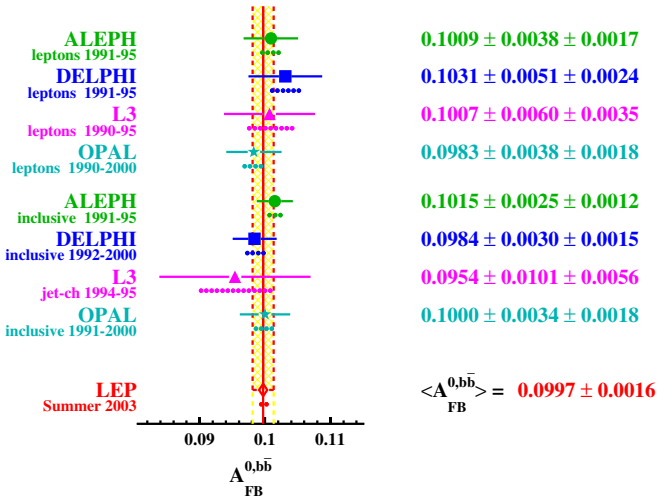

Fig. 3. Measurements of $A_{\rm FB}^{0,\,\rm b}$ using lepton and inclusive tags

The variation of $\mathcal{A}_{\rm f}$ with the value of $\sin^2\theta_{\rm eff}^{\rm lept}$ is shown in Fig. 1. The Z pole asymmetries are related to $\mathcal{A}_{\rm f}$ by:

$$A_{\rm FB}^{0,\,\rm f} = \frac{3}{4}\mathcal{A}_{\rm e}\mathcal{A}_{\rm f}\,;\; A_{\rm LR}^{0} = \mathcal{A}_{\rm e}\,;\; A_{\rm LRFB}^{0} = \frac{3}{4}\mathcal{A}_{\rm f}\,.$$

As a result of the large value of $\mathcal{A}_{\rm b}$ and the fast variation of $\mathcal{A}_{\rm e}$ with $\sin^2\theta_{\rm eff}^{\rm lept}$, $A_{\rm FB}^{0,\,\rm b}$ is particularly sensitive to $\sin^2\theta_{\rm eff}^{\rm lept}$.

2.1 Heavy flavour forward-backward asymmetry measurements

The analyses use Z to hadron decays. The quark direction is approximated by the event thrust axis. Heavy flavours are tagged by leptons with high momentum p or transverse momentum $p_{\rm t}$, by the resolvable heavy hadron lifetimes and by other variables such as the invariant mass of particles associated to a secondary vertex. Forward and backward events are distinguished by the lepton charge or an inclusive charge tag. Fits for $A_{\rm FB}^{\rm b\bar{b}}$ (and $A_{\rm FB}^{\rm c\bar{c}}$) are made in bins of flavour purity to the differential distribution $\mathrm{d}\sigma/\mathrm{d}\cos\theta \propto \frac{3}{8}(1+\cos^2\theta) + A_{\rm FB}\cos\theta$.

Experimentally, the most crucial aspect of the analyses is that they are self-calibrated from data for flavour purity, B^0 mixing and the charge mistag rate using double tag methods. The choice of working point results in analyses that are statistics limited rather than systematics limited.

The LEP combined measurements at the Z peak, and ± 2 GeV away are shown in Fig. 2. These are corrected to give pole asymmetries at $\sqrt{s} = M_{\rm Z}$. The individual and LEP combined pole asymmetry measurements are shown in Fig. 3. All heavy-flavour quantities from LEP and SLD are averaged in one combined fit, accounting for correlated errors and interdependences. The overall χ^2/dof is 52.7/91, indicating that the measurement errors may be overestimated. The average pole asymmetry values are:

$$A_{\rm FB}^{0,\,\rm b} = 0.0997 \pm 0.0016\,,$$
$$A_{\rm FB}^{0,\,\rm c} = 0.0706 \pm 0.0035\,.$$

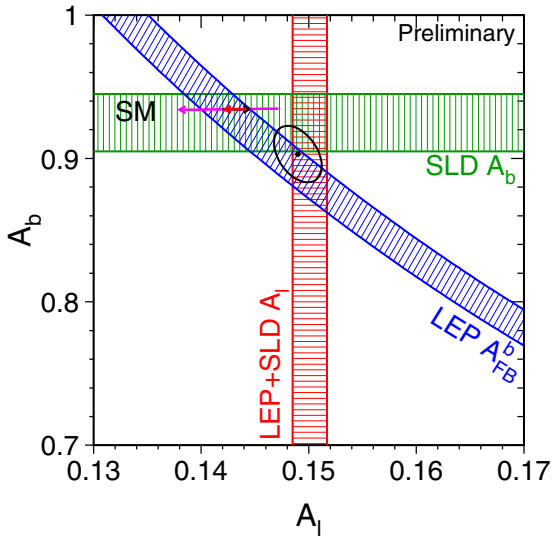

Fig. 4. Constraints on $\mathcal{A}_{\rm b}$ and $\mathcal{A}_\ell$

The total systematic error for the b (c) asymmetries is only 0.0007 (0.0017), of which 0.0004 (0.0009) is a common error to all the measurements. The SM expectations from the best fit to all electroweak data (Sect. 9) are $A_{\rm FB}^{0,\,\rm b} = 0.1036$ and $A_{\rm FB}^{0,\,\rm c} = 0.0740$. The small changes to the average values with respect to summer 2002 are consistent with the improved precision.

2.2 Comparison of asymmetry measurements and $\sin^2\theta_{\rm eff}^{\rm lept}$

The bands in Fig. 4 reflect the direct measurement of $\mathcal{A}_{\rm b}$ from $A_{\rm LRFB}$ at SLD, the combined LEP and SLD knowledge of $\mathcal{A}_\ell$ and the constraint on the product $\mathcal{A}_{\rm e}\mathcal{A}_{\rm b}$ from the forward-backward asymmetry. The SM expectation is indicated by the arrow, which spans a Higgs mass range from 114 to 1000 GeV. The interpretation in terms of $\sin^2\theta_{\rm eff}^{\rm lept}$ is shown in Fig. 5. The χ^2 probability for the

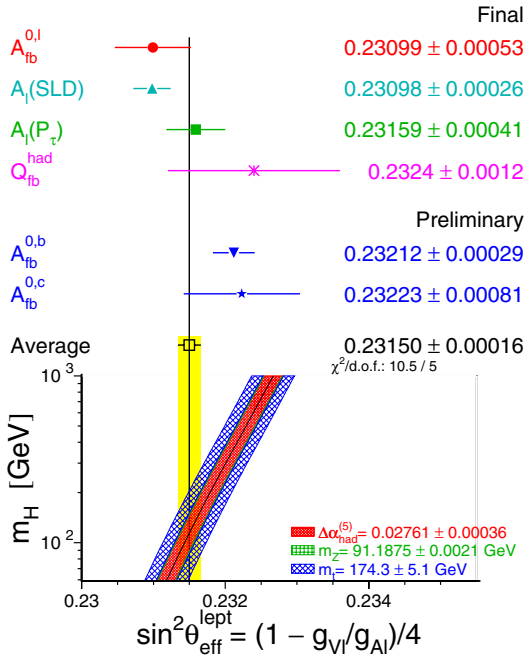

Fig. 5. LEP and SLD measurements of $\sin^2\theta^{\rm lept}_{\rm eff}$

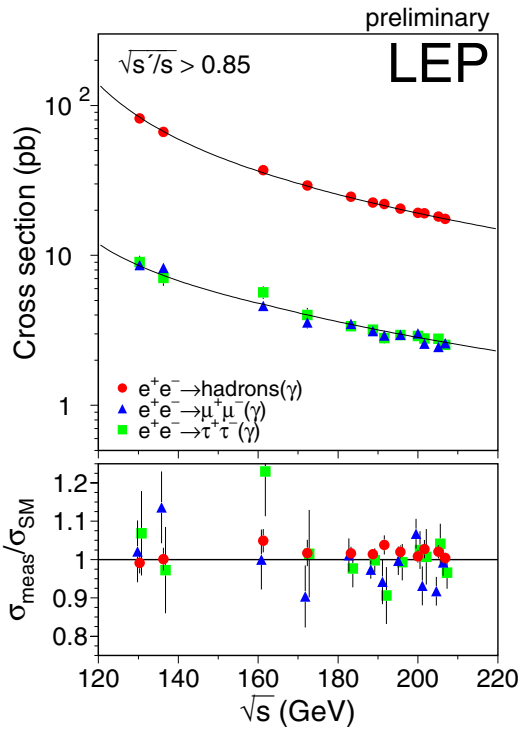

Fig. 7. LEP combined results for two-fermion production

combined value is 6.2%. The two most precise results, from $A_{\rm FB}^{0,\,b}$ and $A_{\rm LR}$, which are both statistics limited, differ by 2.9σ.

3 Fermion pair production at LEP2

The centre-of-mass energies at LEP2 ranged from 161 to 209 GeV. The e^+e^- annihilation cross-section continues to be dominated by fermion-pair production at these energies. The cross-section as a function of the Z/γ propagator mass, $\sqrt{s'}$, shows a characteristic two peaked structure, as seen in Fig. 6. Many events have an energetic initial state photon, bringing the mass of the propagator back to the Z resonance. Two cross-sections are therefore measured, the inclusive cross-section and the cross-section for non-radiative events, defined by $\sqrt{s'/s} > 0.85$. Although OPAL presented updated results at this conference, the LEP combined results, shown for example in Fig. 7, are unchanged since summer 2002 [3]. LEP combined cross-sections, asymmetries and differential cross-sections are available for the following final states: $q\bar{q}$, $b\bar{b}$, $c\bar{c}$, e^+e^-, $\mu^+\mu^-$, $\tau^+\tau^-$. Good agreement with SM predictions is observed. The non-radiative results allow constraints to be made on new physics such as contact interactions or the existence of a Z' boson at energy scales of the order of 1–10 TeV, far above the maximum centre-of-mass energy of the collider.

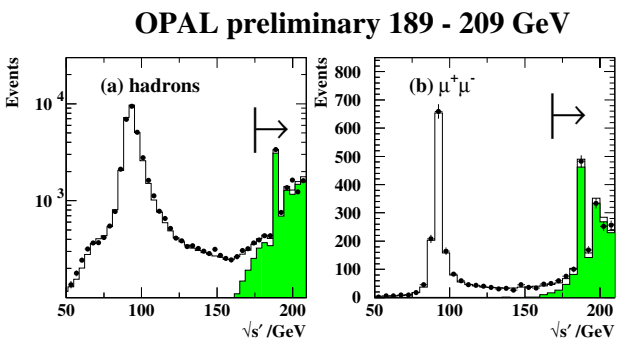

Fig. 6. Number of two-fermion events observed vs. $\sqrt{s'}$

The radiative return peak is at $\sqrt{s'} = M_{\rm Z}$ if the beam energy calibration is correct. The LEP experiments use this feature to check the average beam energy measurement. The measured average beam energy differs from the LEP preliminary value by:

$$\Delta E_{\rm beam} = -14 \pm 21(\text{stat.}) \pm 20(\text{syst.}) \pm 20(\text{LEP})\,\text{MeV}.$$

4 Gauge boson production and decay

4.1 W and Z production at the Tevatron

The two experiments at the Tevatron, CDF and D0, both had major upgrades for Run II, where they are now recording $p\bar{p}$ collisions with $\sqrt{s} = 1.96$ TeV. Run I took place from 1992-1995, when the experiments recorded around 80 pb^{-1} with $\sqrt{s} = 1.8$ TeV. The predictions for integrated luminosity are to record around 300 pb^{-1} in FY2003. Run IIb should deliver between 4.5 (realistic) and 8.5 (optimistic) fb^{-1} by FY2009 [4]. At the time of this conference, the Tevatron had already delivered over 200 pb^{-1} to each experiment. However, the Run II results presented use a partial data set, typically 50 pb^{-1}.

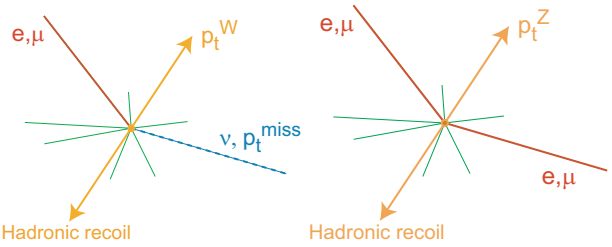

Fig. 8. Characteristics of W and Z production at the Tevatron

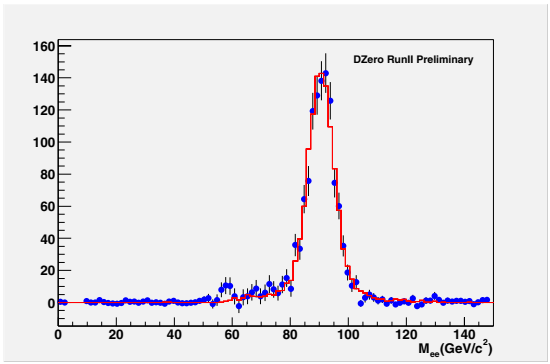

Fig. 9. Mass of Z → ee candidates after background subtraction from 41.6 pb^{-1} of D0 Run II data

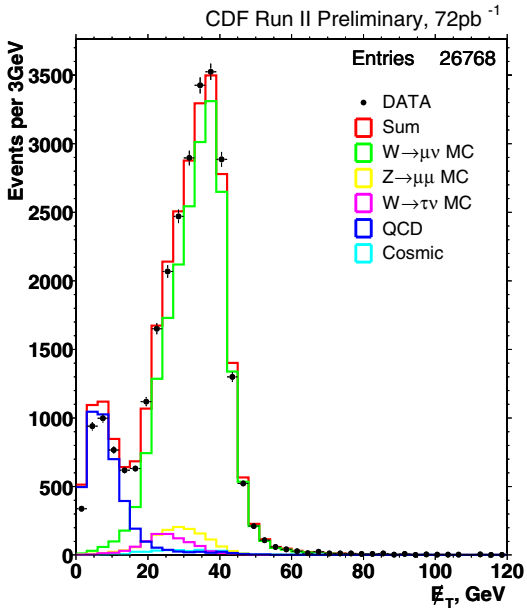

Fig. 10. Missing energy distribution for W → $\mu\nu$ candidates

The processes $q\bar{q}' \to W \to \ell\nu$ and $Z \to \ell^+\ell^-$, where ($\ell = e, \mu$), give very clean signatures, illustrated in Fig. 8. W decays are characterised by an isolated lepton and missing transverse momentum, p_T^{miss}, due to the undetected neutrino. Modelling of p_T^{miss} requires an understanding of the hadronic recoil system. Z decays to two isolated leptons can also easily be picked out, but hadronic W or Z decays are hard to distinguish from QCD background. The significant samples already available from Run II are illustrated in Figs. 9 and 10 [5,6].

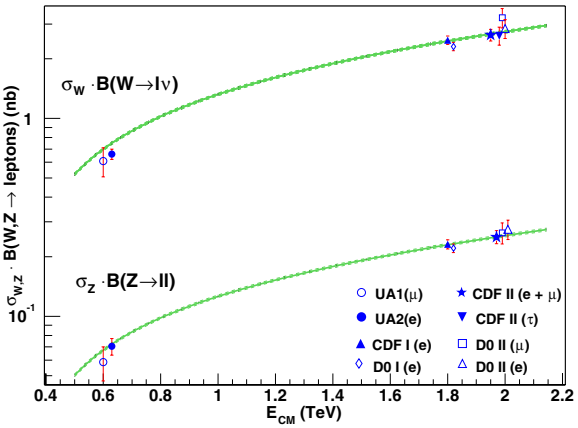

Fig. 11. Gauge boson production cross-section × leptonic Br

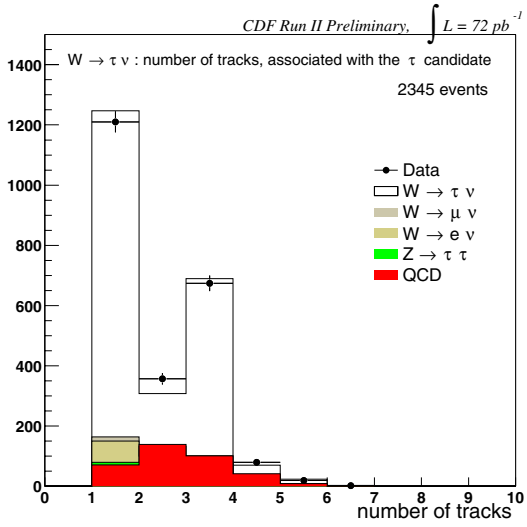

Fig. 12. Number of tracks in τ candidate jets

The experiments measure the cross-section times branching ratio $\sigma_{W,Z} \cdot Br(W, Z \to \text{leptons})$ [5,6]. The results from Run I and Run II are summarised in Fig. 11. Tau-leptons from W decay are identified from the track multiplicity of narrow jets (see Fig. 12). The latest CDF preliminary Run II result testing lepton universality in W decays is $g_\tau/g_e = 0.99 \pm 0.04$.

4.2 Gauge boson production at LEP2

Each of the four experiments observed about 10 thousand W-pair events at LEP2. The lowest order diagrams for WW and ZZ production are shown in Fig. 13. The LEP combined WW and ZZ production cross-sections [7] are shown in Fig. 14. The W-pair cross-section is sensitive to the WWγ and WWZ triple gauge couplings (TGC). At threshold, the cross-section is also sensitive to the exact value of the W mass, but with only 10 pb^{-1} of data the measurement is not very precise. The ZZ cross-section is significantly lower. Nonetheless, ZZ events where one Z decays to $b\bar{b}$ form an irreducible background to the SM Higgs search if the Higgs mass is close to the Z mass.

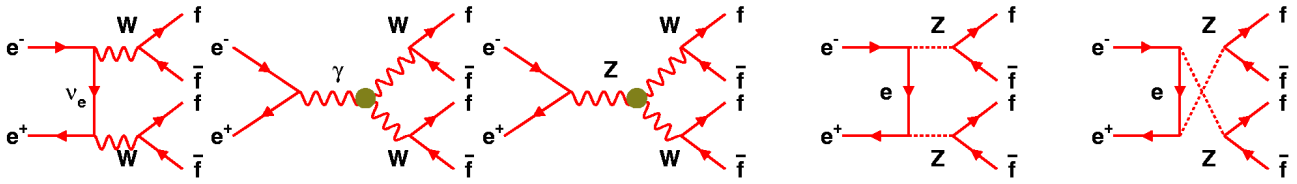

Fig. 13. Three "CC03" diagrams for W pair production and two "NC02" diagrams for Z pair production. The triple gauge couplings are marked in the two s-channel W-pair production diagrams

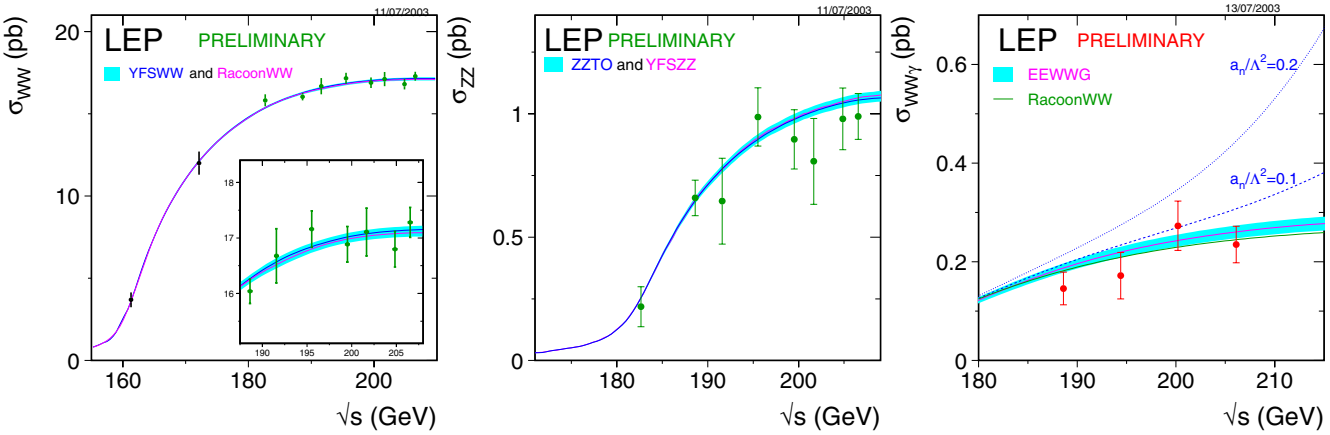

Fig. 14. WW, ZZ and WWγ production cross-sections

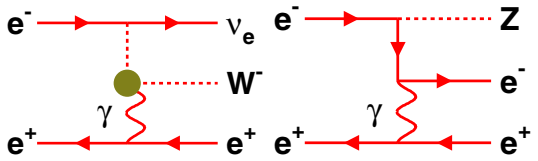

Fig. 15. Examples of "single W" and "single Z" production

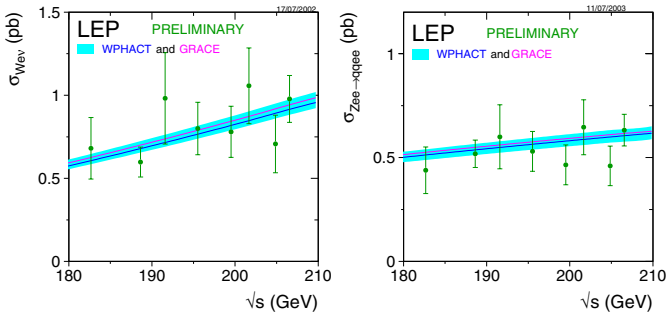

Fig. 16. Cross-sections for single W and single Z production

The three boson final state WWγ has also been studied [7], see Fig. 14. This is dominated by ISR and FSR processes, but is also sensitive to anomalous quartic gauge couplings (QGC). Single production of heavy gauge bosons, $e^+e^- \to e\nu W$ and eeZ, has also been observed [8]. Typical production processes are shown in Fig. 15, and the measured cross-sections in Fig. 16.

Good agreement between all the measured cross-sections and the SM expectation is observed. The WW cross-section is the most precisely measured, with a relative precision of 1%.

4.3 W branching ratios

All the W final states can be measured at LEP2. About 46% of W pair events decay to $q\bar{q}q\bar{q}$, with 4 jets in the final state, and 44% are semileptonic final states, $q\bar{q}\ell\nu$, with 2 jets, a charged lepton and missing momentum, $p^{\rm miss}$. The remaining 10% are fully leptonic, with two charged leptons and $p^{\rm miss}$. The LEP measurements of the W leptonic branching ratios are listed in Fig. 17 [7]. The value for $\mathrm{Br}(\mathrm{W} \to \tau\nu)$ is higher than the SM expectation. As the experiments finalise this measurement, it will be interesting to see if the significance increases or decreases. The corresponding hadronic branching fraction is

$$\mathrm{Br}(\mathrm{W} \to \mathrm{q\bar{q}}) = (67.77 \pm 0.28)\% \,,$$

which can be interpreted as a value of the CKM matrix element squared $|V_{\rm cs}|^2 = 0.989 \pm 0.014$ [7].

The Tevatron experiments measure the product of the W and Z production cross-sections and leptonic branching ratios [5,6,9]. The ratio of these partial cross-sections is

$$R \equiv \frac{\sigma_{\rm W} \cdot \mathrm{Br}(\mathrm{W} \to \ell\nu)}{\sigma_{\rm Z} \cdot \mathrm{Br}(\mathrm{Z} \to \ell\ell)} = \frac{\sigma_{\rm W}}{\sigma_{\rm Z}} \frac{\Gamma_{\rm Z}}{\Gamma(\mathrm{Z} \to \mathrm{ee})} \frac{\Gamma(\mathrm{W} \to \mathrm{e}\nu)}{\Gamma_{\rm W}}$$

The new CDF and D0 combined measurement of R from Run II is $R = 10.36 \pm 0.31$. This can be used to derive a value of $\mathrm{Br}(\mathrm{W} \to \ell\nu)$ or an indirect measurement of the W width $\Gamma_{\rm W}$. The value of $\mathrm{Br}(\mathrm{Z} \to \ell\ell)$ is taken from LEP measurements, the SM value of $\Gamma(\mathrm{W} \to \mathrm{e}\nu)$ is assumed, and the ratio of cross-sections $\sigma_{\rm W}/\sigma_{\rm Z}$ is taken from the theoretical calculation of Van Neerven and Zijlstra [10]. The R value is combined with the Run I measurement,

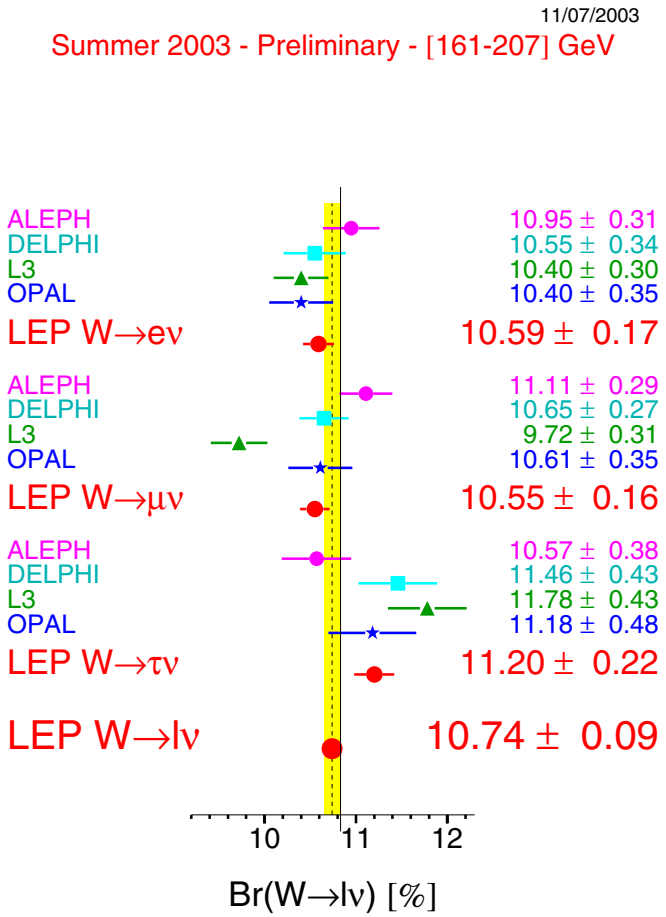

Fig. 17. W leptonic branching ratios

correcting for the evolution of $\sigma_{\rm W}/\sigma_{\rm Z}$ with $\sqrt{s}$. The results are

$$\mathrm{Br}(\mathrm{W} \to \ell\nu) = (10.53 \pm 0.26)\%\,,$$
$$\Gamma_{\rm W} = 2.150 \pm 0.054\,\mathrm{GeV}\,.$$

5 Electroweak tests with gauge bosons

5.1 Examples from the Tevatron

A variety of tests of the structure of the SM can be made with gauge bosons. Continuing with the Tevatron [5], the di-electron forward-backward asymmetry as a function of the mass of the electron pair is shown in Fig. 18. The measurement extends far above LEP energies, but is not competitive with LEP in the region of the Z pole with the present statistics. With a very large data sample $\sin^2\theta^{\rm lept}_{\rm eff}$ could potentially be measured precisely.

The Tevatron experiments also study multi-boson production [5]. The easiest channel is Wγ production, where CDF have observed 81 events, with 25.4 expected background in the e and μ channels combined. Wγ, Zγ, WW and WZ production are sensitive to anomalous TGCs, but at present, LEP results generally give stronger constraints.

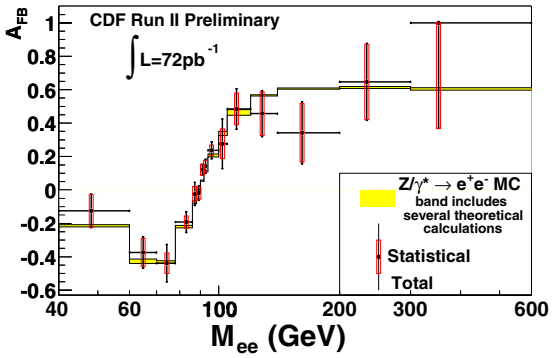

Fig. 18. Dielectron forward-backward asymmetry vs. $M_{\rm e^+e^-}$

5.2 Charged triple gauge couplings at LEP2

There are 14 possible triple gauge couplings, 7 each for WWγ and WWZ. These can be reduced to 5 couplings by imposing EM gauge invariance, CP, C & P conservation. These are: $g_1^{\rm z}$, κ_γ and $\kappa_{\rm z}$, all equal to 1 in the SM; λ_γ and $\lambda_{\rm z}$, equal to 0 in the SM. Imposing SU(2)×U(1) gauge relations makes a further reduction to 3 possible anomalous couplings (where Δ indicates the deviation from the SM expectation): $\Delta\kappa_\gamma$, $\Delta g_1^{\rm z}$ and λ_γ, with $\Delta\kappa_{\rm z} = \Delta g_1^{\rm z} - \Delta\kappa_\gamma \tan^2\theta_W$ and $\lambda_{\rm z} = \lambda_\gamma$.

Anomalous TGCs would change the W helicities and the production and decay angular distributions. For example, the W polarised differential cross-section would be modified from their SM expectation. Measurements have been made at LEP2 [11]. A common technique is to project out spin density matrix elements from the lepton decay-angle distributions in the W restframe. CP and CPT tests can also be made using off-diagonal SDM elements. The measured fractions of longitudinally polarised W's are given in Table 1.

In addition, direct fits for anomalous TGCs have been performed [12] using WW, single W and single γ events.

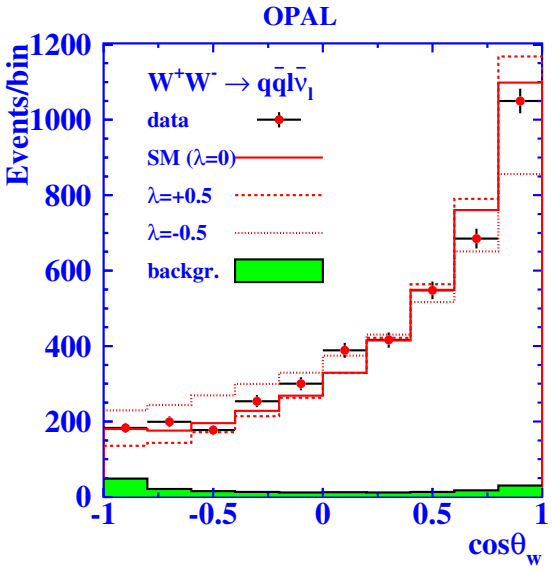

Fig. 19. Distribution of the W production angle

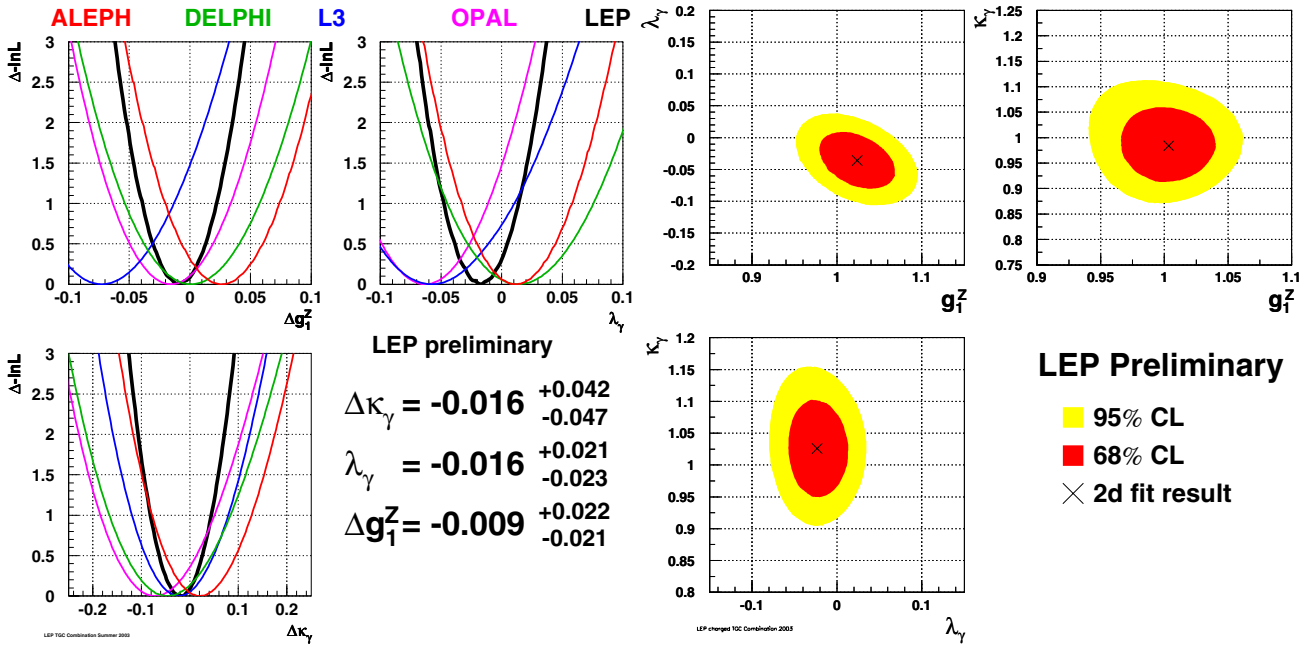

Fig. 20. Results of 1d (*left*) and 2d (*right*) fits for triple gauge couplings

Table 1. Fraction of longitudinally polarised W bosons

	σ_L/σ_{tot}
DELPHI	(24.9 ± 3.2) %
L3	$(21.8 \pm 2.7 \pm 1.6)$ %
OPAL	$(23.8 \pm 2.1 \pm 1.4)$ %
SM	23.9 ± 0.1 %

In general, differential cross-sections give stronger constraints than total cross-sections. The most sensitive single variable is $\cos\theta_W$, the W production angle in W-pair events. "Optimal observables" can be constructed to exploit the full information from the event sample, including correlations between angular variables. Fits are made allowing one, two or three coupings to vary at the same time, see Fig. 20. The LEP results are combined at the level of likelihood curves for the anomalous couplings, rather than by trying to fit to combined angular distributions [12]. The couplings are measured to a precision of a few %, and are found to be consistent with the SM expectation.

5.3 Neutral TGC

There are no neutral triple gauge couplings in the SM. Searches for anomalous neutral TGCs examine the $Z\gamma$ and ZZ cross-sections and differential distributions. Parametrizations exist of two types of anomalous vertex, assuming that the final state bosons are on shell. Results given here are LEP combined results at 95% CL from fits where only one coupling is free at a time.

The process $e^+e^- \to Z\gamma$ by s-channel Z/γ exchange would involve anomalous $Z\gamma\gamma$ or $ZZ\gamma$ vertices. Events with $Z \to q\bar{q}$ or $\nu\bar{\nu}$ are studied. The dominant background is from ISR. Constraints may be placed on 4 couplings $|h_i^\gamma| \lesssim 0.05$ and 4 couplings $|h_i^Z| \lesssim 0.15$.

To produce two on-shell Z bosons in the final state, from $e^+e^- \to ZZ$ by s-channel Z/γ exchange would require $ZZ\gamma$ or ZZZ vertices. Examination of ZZ events allows constraints to be placed on 4 couplings $|f_{4,5}^{\gamma,Z}| \lesssim 0.4$ [12].

5.4 Quartic gauge couplings

Quartic vertices WWWW, WWZZ, WWZγ and WW$\gamma\gamma$ exist in the SM, although they give only small contributions at LEP2. The experiments have investigated possible anomalous QGCs that respect TGCs [12]. Example processes are illustrated in Fig. 21. The main backgrounds arise from single or double ISR. No deviations from the SM expectation have been reported.

6 W mass and width

6.1 W mass measurement at LEP

The W mass at LEP2 is measured by fitting the distribution of W masses reconstructed from final state particles, using all the data recorded above threshold [13]. The W width is either fixed to the expected value from the precise SM relation between Γ_W and M_W or fitted from the data.

For the semileptonic final state, $q\bar{q}\ell\nu$, the neutrino momentum must be inferred from the rest of the event. However, there is no ambiguity in assigning particles to the parent W. In contrast, there is an important combinatorial background in the $q\bar{q}q\bar{q}$ channel, which can be reduced by jet pairing likelihoods, for example. Some analyses allow

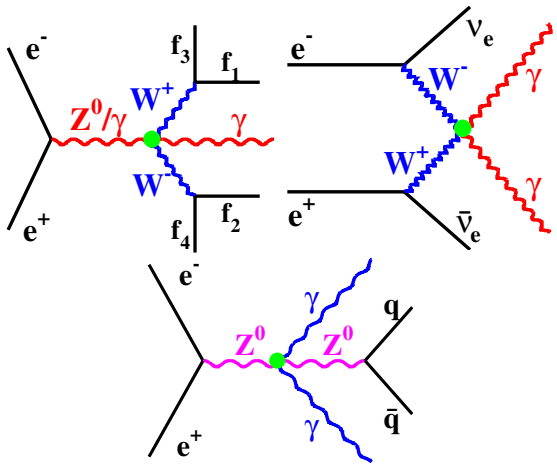

Fig. 21. Diagrams with a quartic gauge coupling

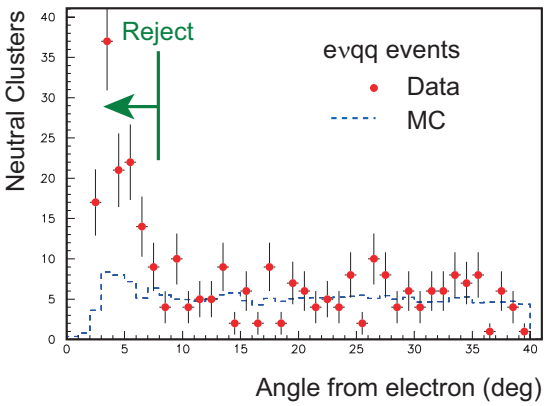

Fig. 22. Distribution of neutral clusters as a function of angle from the electron candidate in ALEPH

5 jets in the final state to account for hard gluon radiation. The $\ell\nu\ell\nu$ channel has lower statistics and two missing neutrinos. Nonetheless, there is some sensitivity to the W mass from the lepton energy E_ℓ and other kinematic variables. The statistical error is about 10 times larger than for the other channels.

Kinematic fits are used to improve significantly the mass resolution, imposing energy and momentum conservation, and optionally requiring that the two W masses are equal. As a result the W mass picks up a systematic uncertainty from the knowledge of the LEP beam energy: $\delta M_{\rm W}/M_{\rm W} \approx \delta E_{\rm beam}/E_{\rm beam}$.

The result from ALEPH was updated in 2003, with a shift of -79 MeV to 80.385 ± 0.059 GeV. The change was due to a problem in simulating shower satellites in the electromagnetic calorimeter. These satellites are low energy neutral clusters. An excess of clusters was seen, especially near electrons. Extra clusters that should have been included with the electron bias the direction of jets in the event. More generally, jet masses are biassed by the extra clusters. The problem was addressed by an improved shower simulation with the EGS Monte Carlo, and by rejecting "single stack" neutral clusters (i.e. clusters in a single calorimeter element), a process dubbed

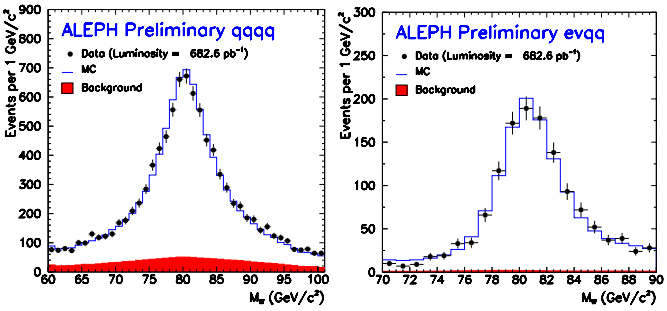

Fig. 23. Example distributions of reconstructed W mass

Table 2. Dominant errors in the LEP combined W mass

Error (MeV)	$\mathrm{q\bar{q}}\ell\nu$	$\mathrm{q\bar{q}q\bar{q}}$	Both
ISR/FSR	8	8	8
Hadronisation	19	18	18
Detector	14	10	14
LEP Beam Energy	17	17	17
Colour Reconnection	–	90	9
Bose-Einstein	–	35	3
Total Systematic	31	101	31
Statistical	32	35	29

"cleaning". After this, a discrepancy remains, as shown in Fig. 22. The impact of this discrepancy is minimised by rejecting neutral clusters within 8 degrees of an electron at the calorimeter entrance. This requirement retains Bremsstrah-lung photons, which arrive at the calorimeter futher away.

No evidence of any similar problem has been found by the other LEP experiments. Example $M_{\rm W}$ distributions for the $\mathrm{q\bar{q}q\bar{q}}$ and $e\nu\mathrm{q\bar{q}}$ final states are shown in Fig. 23.

6.1.1 LEP W mass systematic uncertainties

The dominant systematic uncertainties in the W mass measurement are given in Table 2. Although the statistical uncertainty in the W mass from the hadronic and semileptonic final states is about the same, important systematic uncertainties due to final state interactions in the $\mathrm{q\bar{q}q\bar{q}}$ channel result in it having a weight of less than about 10 % in the combination.

In general, the two W boson decay vertices are separated by about 0.1 fm, but the typical hadronic distance scale is about 1 fm. Even small changes to the flow of soft particles between jets from different W bosons can change the reconstructed W mass by several tens of MeV. Colour reconnection concerns a rearrangement of colour flow, either in the parton shower or during the hadronisation process. Bose-Einstein correlations between like-sign identical bosons also change the distribution of soft particles. Controlling these two effects is vital to achieving the best possible measurement of the W mass from the LEP2 sample.

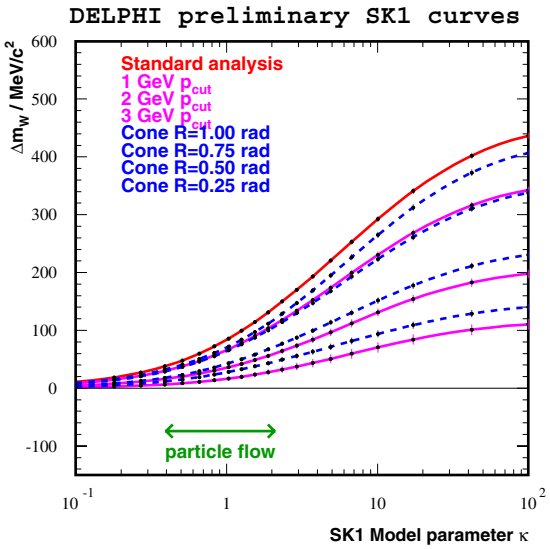

Fig. 24. Change in the W mass as a function of the amount of colour reconnection

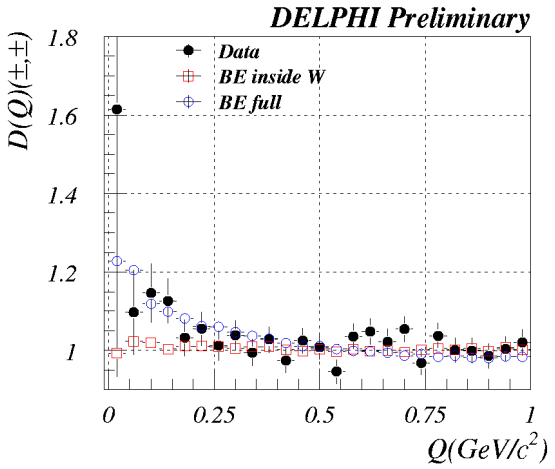

Fig. 25. The ratio $D(Q)$ in the low Q^2 region for like sign pairs in data, compared with Monte Carlo with BEC only in the same W, and full BEC

6.1.2 Colour reconnection in the $q\bar{q}q\bar{q}$ final state

The uncertainty due to colour reconnection (CR) [14] is assessed by using different Monte Carlo models. These include SK-I, which has a free parameter κ that controls the fraction of CR, and ARIADNE-II and HERWIG.

The particle flow method looks at the number of particles between jets from the same W and jets from different W's. In the case of CR between different W's, the number of particles between jets from different W's increases. Particle flow measurements have restricted the range of the SK-I parameter κ. This range sets the present error on M_{W}.

A new method is referred to as "cuts and cones" [14]. The W mass is evaluated after determining some or all of the jet properties excluding low momentum particles, "cuts", or with a cone jet-finder which excludes particles furthest from the jet core. When this procedure is repeated with different CR models, the shift in the W mass due to CR is reduced, see Fig. 24. However, the statistical uncertainty in the W mass increases, due to the loss of information. Comparing the W mass shift as a function of the momentum cut or cone radius in data and Monte Carlo samples further constrains CR models. The intention is to use this method for the final LEP W mass measurement, choosing a cut or cone working point that minimises the total error.

6.1.3 Bose-Einstein correlations

Although Bose-Einstein correlations (BEC) are well established in Z decays, for example, it is not clear whether they occur between identical bosons from different W bosons [15]. The present error on the W mass due to BEC is assessed from the full effect of the LUBOEI model to be $\delta M_{\mathrm{W}} = 35$ MeV.

The LEP experiments have looked for evidence of BEC between W decays in the data. For completely independent W decays, the inclusive two-particle density in $q\bar{q}q\bar{q}$ events as a function of the 4-momentum difference of the particles, $Q^2 = (p_1 - p_2)^2$, is given by:

$$\rho^{\mathrm{WW}}(Q)_{\mathrm{indep}} = 2\rho^{\mathrm{W}}(Q) + 2\rho^{\mathrm{WW}}_{\mathrm{mix}}(Q)$$

Here $\rho^{\mathrm{W}}(Q)$ is the two-particle density of a single W, and $\rho^{\mathrm{WW}}_{\mathrm{mix}}$ is constructed by mixing the $q\bar{q}$ parts of two different $q\bar{q}\ell\nu$ events. This can be compared with the true two-particle density, observed in data, either by looking at the difference, $\Delta\rho(Q) = \rho^{\mathrm{WW}}(Q) - \rho^{\mathrm{WW}}(Q)_{\mathrm{indep}}$ or the analogous ratio $D(Q)$. These variables are checked for like and unlike sign pairs. Data is compared with Monte Carlo samples including no BEC, BEC only between bosons from the same W, and full BEC.

An example from DELPHI is shown in Fig. 25, where the data prefer the full BEC model. However, the other experiments measurements prefer BEC only between the decay products of the same W. This is illustrated in Fig. 26. The results are parametrised by the observed fraction of the BEC model between identical bosons from different W bosons. The combined result constrains the fraction to be less than 0.36 at 68% CL, which would reduce the uncertainty on the W mass due to BEC from 35 to 13 MeV.

6.1.4 Combined W mass from LEP

The preliminary results from the LEP experiments are given in Fig. 27. Note that the OPAL result does not yet include data from the last year of LEP running. The W mass measured at LEP,

$$M_{\mathrm{W}} = 80.412 \pm 0.029(\mathrm{stat.}) \pm 0.031(\mathrm{syst.})\,\mathrm{GeV},$$

prefers a low value of the Higgs mass in the SM. The new ALEPH result shifted the LEP average by -35 MeV, increasing the preferred Higgs boson mass.

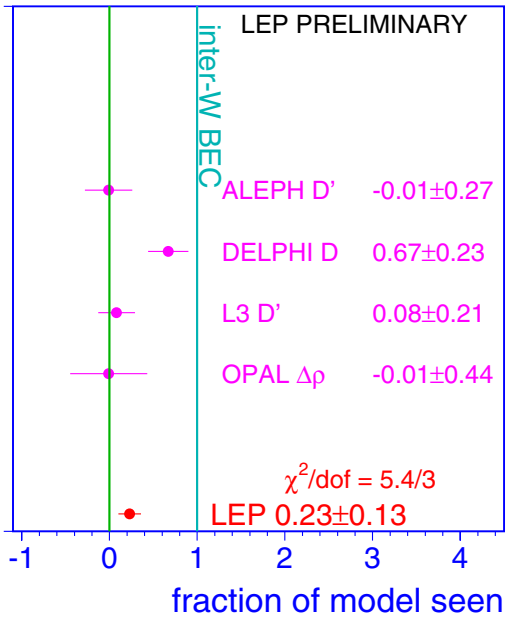

Fig. 26. Observed fractions of the full BEC model

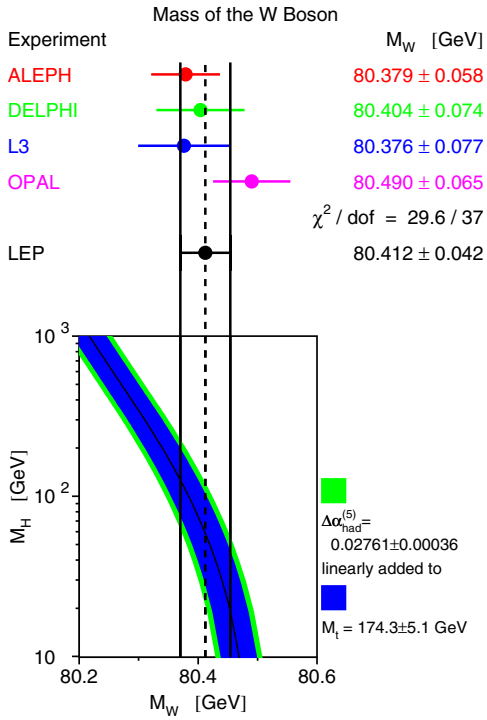

Fig. 27. W mass measurements from LEP

As a cross-check, the difference is calculated between the results from the semileptonic and hadronic channels, setting the CR and BEC uncertainties to zero. The difference is consistent with zero: $\Delta M_{\rm W} = +22 \pm 43$ MeV.

6.2 W mass from Tevatron

The Run I W mass results are final [9]. The W mass is derived from a fit to the Jacobian edge of the transverse

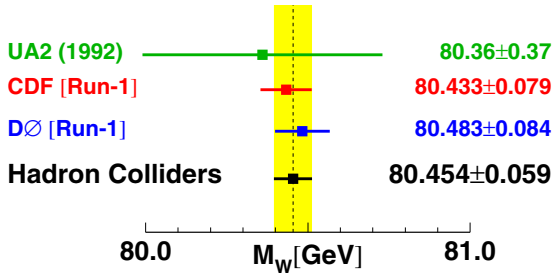

Fig. 28. W mass measurements from hadron colliders

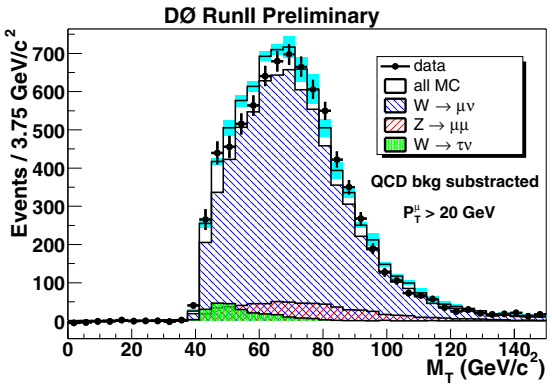

Fig. 29. Transverse mass distribution of $\mathrm{W} \to \mu\nu$ events

mass distribution, and the width from the high mass tail, where the transverse mass is given by

$$M_{\rm T}^2 = 2p_{\rm T}^{\ell} p_{\rm T}^{\nu} (1 - \cos(\phi^{\ell} - \phi^{\nu})) \,.$$

D0 also fit the $p_{\rm T}^{\ell}$ and $p_{\rm T}^{\rm miss} = p_{\rm T}^{\nu}$ distributions and quote a combined result.

The average W mass value from the Tevatron Run I and from UA2 is

$$M_{\rm W} = 80.454 \pm 0.059\,\mathrm{GeV} \,.$$

No new result has been reported from Run II. An example of the Run II data quality is shown in Fig. 29. Systematic errors on the W mass from the Tevatron will be reduced with more luminosity. In particular, the energy and momentum scales are controlled with Z events (and $\mathrm{J}/\psi, \Upsilon, \pi^0$) and the response to the hadronic recoil and the $p_{\rm T}^{W}$ model are also constrained by Z data.

6.3 World average W mass and width

As shown in Fig. 30, the world average values of the W mass and width are

$$M_{\rm W} = 80.426 \pm 0.034\,\mathrm{GeV} \,,$$
$$\Gamma_{\rm W} = 2.139 \pm 0.069\,\mathrm{GeV} \,.$$

These can be compared with various indirect results. The predictions from electroweak fits to LEP1 and SLD data and to the top mass measurement are discussed in Sect. 9. The indirect measurement of the width from hadron colliders was explained in Sect. 4.3. The NuTeV experiment

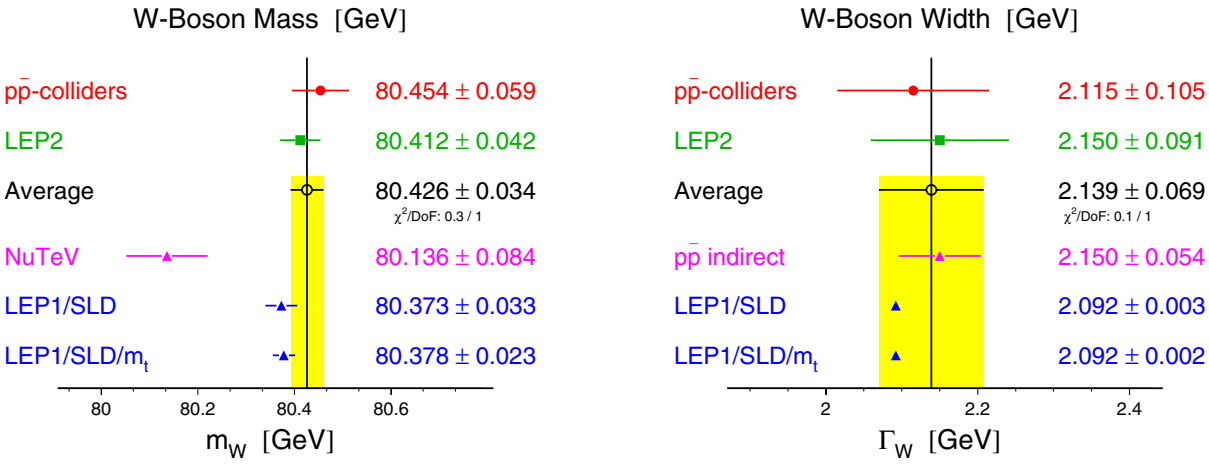

Fig. 30. Summary of W mass and width measurements

measures CC and NC rates for ν_μ and $\overline{\nu}_\mu$ beams. These are related to the W and Z mass ratio via $\sin^2\theta_W = 1 - M_W^2/M_Z^2$ by the Paschos-Wolfenstein relation. There are no new proposals [16] to explain the 3.0σ discrepancy between the SM prediction and the measured value of $\sin^2\theta_W = 0.22773 \pm 0.00135(\text{stat.}) \pm 0.00093(\text{syst.})$.

7 Top physics

7.1 Top quark production at Tevatron

The dominant production mechanism (90%) for top quarks at the Tevatron is $q\overline{q} \to t\overline{t}$ by s-channel gluon exchange. Each top decays to a W boson and a bottom quark. The event topologies depend on the two W decays, see Fig. 31. In the lepton plus jets channel, one W decays

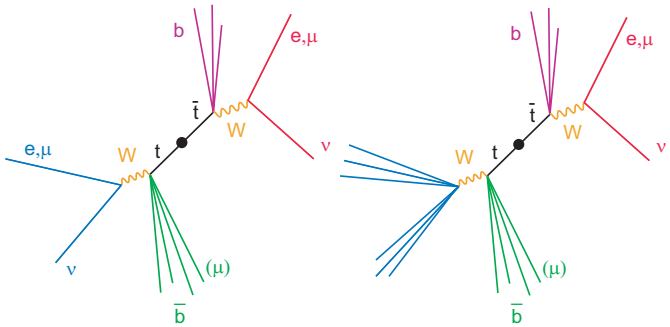

Fig. 31. Di-lepton and lepton plus jets $t\overline{t}$ events

to hadrons, the other leptonically. Four jets, a charged lepton and p_T^{miss} are expected in the final state. Applying a soft muon or lifetime tag to select b jets greatly improves the signal to background.

7.2 Run II top cross-sections

First results from Run II on the top quark production cross-section are available [17]. Figure 32 shows CDF results from the lepton plus jets channel with a vertex tag from Run I and Run II. Within the large uncertainties, the results are consistent with the theoretical expectation at the two centre-of-mass energies. Preliminary Run II measurements from D0 are summarised in Fig. 33, with the exception of a new result for this conference using a lifetime b-tag with the upgraded tracking system, illustrated in Fig. 34. This shows the number of jets in events with an impact parameter significance tag. The excess of events with three or four jets is interpretted as the $t\overline{t}$ signal. This result is included in the summary of cross-section measurements in Table 3.

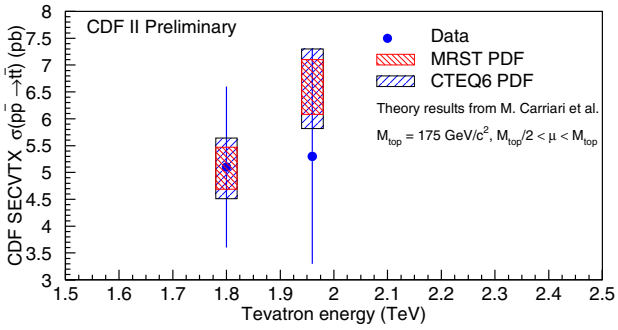

Fig. 32. CDF measurements of the $t\overline{t}$ cross-section

Table 3. Summary of CDF and D0 $t\overline{t}$ cross-section measurements

$\sigma_{t\overline{t}}$ (pb) with stat, syst and lumi errors	
CDF dilepton Run II	$13.2 \pm 5.9 \pm 1.5 \pm 0.8$
CDF ℓ+jets Run II	$5.3 \pm 1.9 \pm 0.8 \pm 0.3$
D0 Run II	$8.4\ ^{+4.5}_{-3.7}\ ^{+6.3}_{-3.5} \pm 0.8$
D0 IP b-tag	$7.4\ ^{+4.4}_{-3.6}\ ^{+2.1}_{-1.8} \pm 0.7$

7.3 Top quark mass

There are two recent results on the top quark mass. D0 have reanalysed the lepton plus jets data from Run I [18].

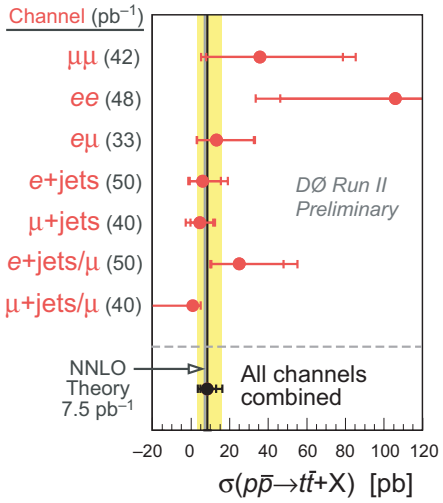

Fig. 33. Measurements of the $t\bar{t}$ cross-section from D0. The

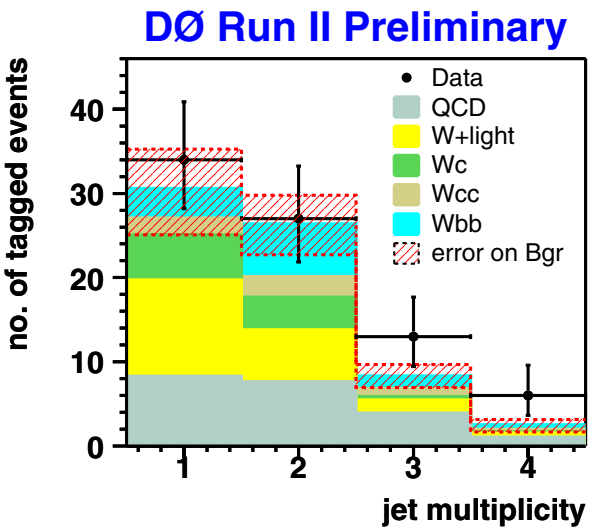

Fig. 34. Number of jets in b-tagged events in 45 pb^{-1} data from Run II

The original publication [19] used 77 events (29 signal and 48 background) in this channel. Of these, 22 events (10 signal, 12 background) have been reanalysed using individual event probabilities instead of the same mass template for all events. It was found to be an advantage to use only the most signal-like events, hence the smaller data sample. In an ensemble of toy MC experiments using the same luminosity as the data sample, the width of the distribution of fitted top masses is reduced from 8.0 to 4.8 GeV. This new result,

$$m_{\mathrm{t}} = 180.1 \pm 3.6(\mathrm{stat.}) \pm 4.0(\mathrm{syst.})\,\mathrm{GeV}\,,$$

is of comparable precision to the old CDF plus D0 average, see Fig. 35.

CDF also reported a preliminary number [20] from lepton plus jets events in Run II with large statistcal and systematic errors (due to the preliminary detector calibration): $171.2 \pm 13.4(\mathrm{stat.}) \pm 9.9(\mathrm{syst.})$ GeV.

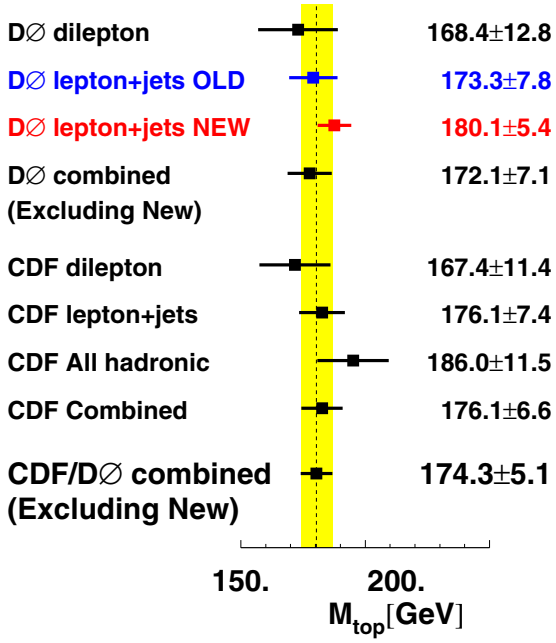

Fig. 35. Top quark mass measurements. The previous world average is shown, and the old and new D0 results are compared

8 Muon $(g-2)$ and $\alpha(M_{\mathrm{Z}}^2)$

8.1 Anomalous magnetic moment of the muon

The Muon $(g-2)$ Collaboration at the Brookhaven AGS measure the muon spin precession frequency in a precisely known magnetic field. In 2002 they inferred the anomalous magnetic moment of the positive muon, $a_\mu = (g-2)/2$ to a precision of 0.7 ppm using data recorded up to the year 2000 [21]:

$$a_\mu = 11\,659\,203(8) \times 10^{-10}\,.$$

A data sample of similar size with μ^- was recorded in 2001, but no new result has been released to date.

The theoretical prediction for a_μ is in poor agreement [22]. In addition, the predictions have a large spread, see Fig. 36. Many groups have contributed to the prediction of a_μ, which includes the following terms:

$$a_\mu^{\mathrm{SM}} = a_\mu^{\mathrm{QED}} + a_\mu^{\mathrm{had,LO}} + a_\mu^{\mathrm{had,HO}} + a_\mu^{\mathrm{had,LBL}} + a_\mu^{\mathrm{weak}}$$

Feynman diagrams illustrating each term are shown in Fig. 37, and the calculated sizes and uncertainties are listed in Table 4. The largest contribution is from QED, but this term is rather precisely known, being calculated to the 5-loop level. The next largest contribution is from the lowest order graph with a hadronic loop of any kind. This is the term for which the predictions from different groups have a spread larger than the uncertainty of about 6×10^{-10} quoted by any one group. The expected contribution from hadronic light-by-light scattering graphs changed sign in recent years, giving the largest change in the prediction. This term has the next largest uncertainty. Electroweak corrections have been calculated at 2-loop level.

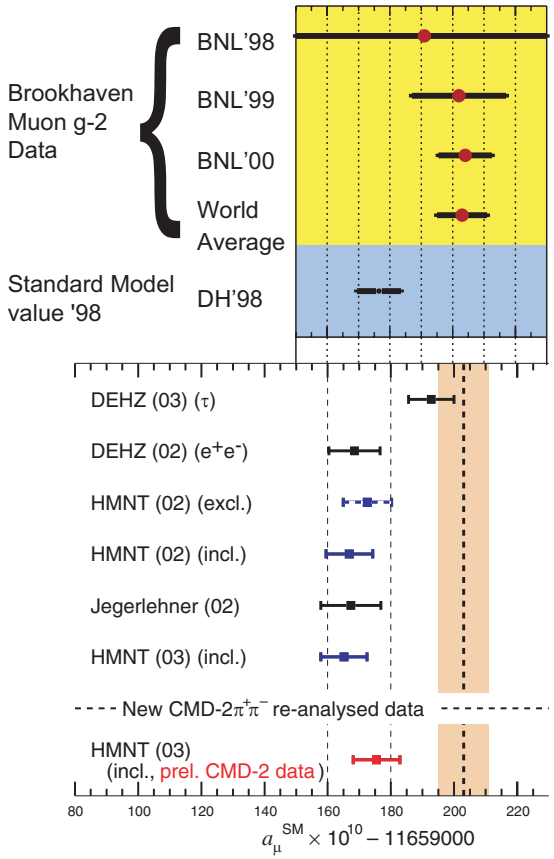

Fig. 36. Comparison of measurements and predictions for the muon anomalous magnetic moment

The calculation of $a_\mu^{\rm had,LO}$ relies on e^+e^- collision data via the dispersion integral

$$a_\mu^{\rm had,LO} = \frac{1}{4\pi^3}\int_{4m_\pi^2}^{\infty} \sigma^0_{\rm had}(s)K(s){\rm d}s\,,$$

where $\sigma^0_{\rm had}$ is the bare cross-section for $e^+e^- \to$ hadrons, i.e. taking out radiative corrections. The QED kernel $K(s) \sim m_\mu^2/3s$, gives the highest weight to the lowest energy data.

Davier *et al.* also include information from τ lepton spectral functions, which are related to e^+e^- annihilation by isospin rotation [23]. The isospin breaking terms are thought to be sufficiently precisely known.

The precision of the predictions has benefitted from the inclusion of recent data, in particular from CMD-2, SND, BES at 2-5 GeV and preliminary ALEPH data on τ spectral functions (combined with existing results from CLEO and OPAL) [22]. The contributions from different centre-of-mass energies are given in Table 5, based on [22, 24]. The largest contributions and uncertainties come from the lowest energy region, where the τ lepton data are most relevant. One of the most difficult aspects of interpreting the data is to know which radiative corrections have been applied, since the bare cross-section is needed. A new preliminary result from CMD-2 released in July 2003 gave a reevaluation of the radiative corrections used in their publication [22]. Finalising these corrections is crucial.

Table 4. Size and uncertainty in contributions to a_μ

	$\Delta a_\mu \cdot 10^{10}$
QED	$(11\,658\,470.35 \pm 0.28)$
had,LO	$(684.7 \text{ to } 709.0 \pm 6)$
had,HO	(-10.0 ± 0.6)
had,LBL	(8.0 ± 4.0)
weak	(15.4 ± 0.2)

Table 5. The largest contributions to $a_\mu^{\rm had,LO}$.

Range/GeV	$\Delta a_\mu^{\rm had,LO} \cdot 10^{10}$
0.32 – 1.43	605.4 ± 5.2
1.43 – 2.00	32.4 ± 2.5
2.00 – 11.09	42.1 ± 1.1

Further differences between the groups include the technique to interpolate between data points, the choice of which older, less precise data to retain, whether to use perturbative QCD between resonances, and difference between the values of $\sigma^0_{\rm had}$ derived from inclusive measurements and from summing over exclusive channels.

Brand new results were shown at this conference from KLOE and Babar using radiative return data to explore lower centre-of-mass energies [25]. The KLOE data prefer the previous e^+e^- annihilation cross-section measurements to those inferred from τ decays.

8.2 Calculation of $\alpha(M_Z^2)$

The value of the electromagnetic coupling constant at the Z mass is a crucial ingredient of global fits to electroweak data. It can be expressed as

$$\alpha(s) = \frac{\alpha(0)}{1 - \Delta\alpha_\ell(s) - \Delta\alpha_{\rm top}(s) - \Delta\alpha^{(5)}_{\rm had}(s)}\,,$$

with $\alpha(0) = 1/137.035\,999\,76(50)$. The hadronic contribution is calculated from a dispersion integral, using similar techniques to the calculation of $a_\mu^{\rm had,LO}$:

$$\Delta\alpha^{(5)}_{\rm had} = -\frac{\alpha s}{3\pi}P\int_{4m_\pi^2}^{\infty}\frac{R_{\rm had}(s'){\rm d}s'}{s'(s'-s)}\,,$$

expressed as a function of the ratio of the hadronic and muon pair final states in e^+e^- annihilation, $R_{\rm had}(s) = \sigma^0_{\rm had}/(\sigma^0_{\mu\mu} = 4\pi\alpha^2/3s)$. Higher centre-of-mass energy data have a larger weight than in the calculation of $a_\mu^{\rm had,LO}$. At present the LEP Electroweak Working Group [26] make global fits using a result by Burkhardt and Pietrzyk, based only on data, of $\Delta\alpha^{(5)}_{\rm had}(M_Z^2) = 0.02761 \pm 0.00036$ [27]. The global fits are repeated using a more precise value that is calculated using perturbative QCD in the continuum region of $\Delta\alpha^{(5)}_{\rm had}(M_Z^2) = 0.02747 \pm 0.00012$ [28]. The

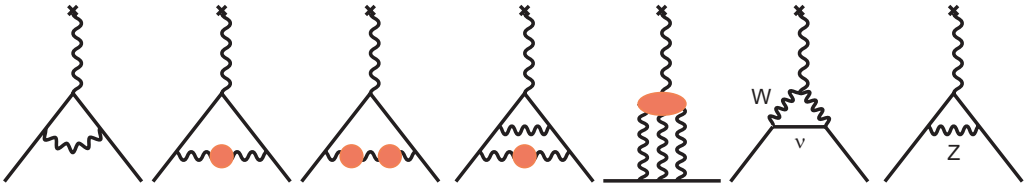

Fig. 37. Example Feynman graphs for each contribution to the prediction of a_μ

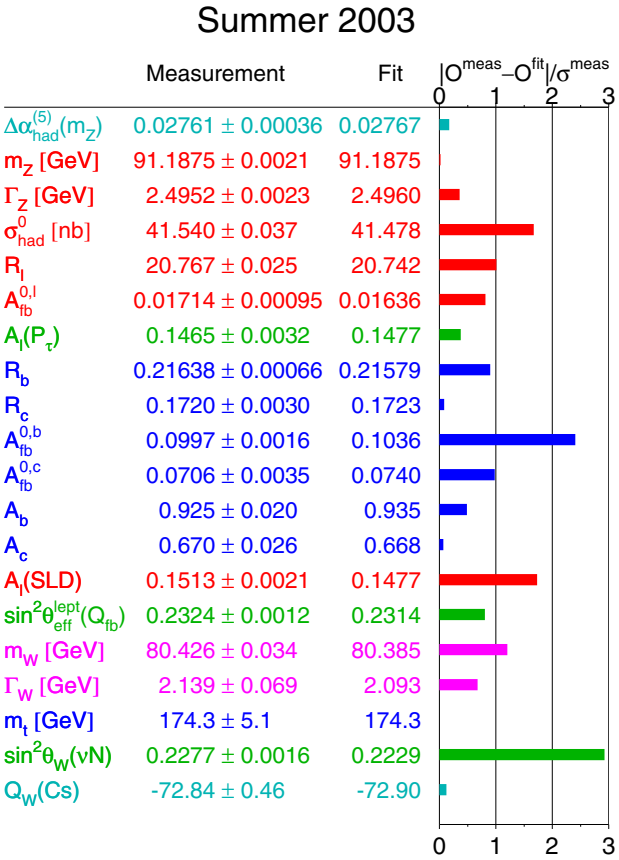

Fig. 38. Compilation of input measurements, best fit values and the corresponding pull for the global electroweak fit to the full set of variables

Burkhardt and Pietrzyk result uses a preliminary CMD-2 [29] which precedes both the publication [30] and the July 2003 preliminary correction to the publication. Using the published value would decrease this estimate of $\Delta\alpha^{(5)}_{\rm had}(M_{\rm Z}^2)$ by 10% of its total uncertainty. However, using the new preliminary reevaluation increases the value by 18% of its total uncertainty to 0.02768 ± 0.00036 [22, 31].

9 Global electroweak fits and the Higgs mass

All electroweak observables can be calculated from a small number of input parameters [32], for example the set

$$\alpha(M_{\rm Z}^2)\,,\ \alpha_{\rm S}(M_{\rm Z}^2)\,,\ M_{\rm Z}\,,\ M_{\rm W}\,,\ m_{\rm t}\,,\ m_{\rm H}\,.$$

Radiative corrections have leading terms in $m_{\rm t}^2$ and $\log m_{\rm H}$. These are calculated using ZFITTER for the LEP Electroweak Working Group fits shown here. $G_{\rm F}$ is known more precisely than $M_{\rm W}$, so it is convenient to change basis and use this as an input instead. The tree level relation is

$$G_{\rm F} \;=\; \frac{\pi\alpha}{\sqrt{2}M_{\rm W}^2\sin^2\theta_{\rm W}} = 1.16639(1)\cdot 10^{-5}\,{\rm GeV}^{-2}\,.$$

The chosen inputs and the other calculated quantities are compared with experimentally measured values in global electroweak fits, to find the best fit values of the input quantities. The measurements used are listed in Fig. 38 [32,26]. They have all been discussed above, except for the measurement of the effective weak charge of Cesium from the level of atomic parity violation, where there has been a recent very small change from an improved calculation of radiative corrections to the result [33].

Fits are made to several subsets of data. Three examples are listed in Table 6. No external $\alpha_{\rm S}$ measurement is used in the fits, and additional theoretical systematic uncertainties are not included at this stage.

The fit to Z pole data allows a comparison of the top and W mass values predicted by radiative corrections and measured directly by LEP2 and the Tevatron, as displayed in Fig. 39. Consistency is seen between the predicted and measured values. The bands predicted by the SM for different values of the Higgs mass are also shown. The data prefer a low value of the Higgs mass.

The χ^2 as a function of Higgs mass from a fit to all the data is shown in Fig 40. The result of a fit excluding the NuTeV result is almost indistinguishable from the central result on this plot, since the NuTeV result has relatively poor precision. However, the fit probability increases from 4.4% to 27.5%. The effect of using the more theoretically motivated value of $\Delta\alpha^{(5)}_{\rm had}(M_{\rm Z}^2)$ is also shown in the figure. Without accounting for the limit from direct searches, but including the spread of theoretical uncertainties, the Higgs mass is constrained to be

$$M_{\rm Higgs} < 219\ \ {\rm GeV\ at\ 95\%\ CL.}$$

The impact of using the preliminary correction to the CMD-2 data, and an indication of the effect the new D0 top mass measurement could have, are shown in Fig. 41. The new value of $\Delta\alpha^{(5)}_{\rm had}(M_{\rm Z}^2)$ [31] leades to a small downward shift in $M_{\rm Higgs}$. The minimum of the curve moves from 96 to 91 GeV, and the 95% CL limit from 219 to 210 GeV. Simply increasing the top mass by 1σ of its present uncertainty to 179.4 ± 5.1 GeV leads to a large upward

Table 6. Results of electroweak fits to three sets of data.

	All Z pole	All data	All but NuTeV
m_t (GeV)	$171.5^{+11.9}_{-9.4}$	$174.3^{+4.5}_{-4.4}$	$175.3^{+4.4}_{-4.3}$
m_H (GeV)	89^{+122}_{-45}	96^{+60}_{-38}	91^{+55}_{-36}
$\alpha_S(M_Z^2)$	0.1187 ± 0.0027	0.1186 ± 0.0027	0.1185 ± 0.0027
χ^2/dof (P)	14.7/10(14.3%)	25.4/15(4.5%)	16.7/14(27.5%)

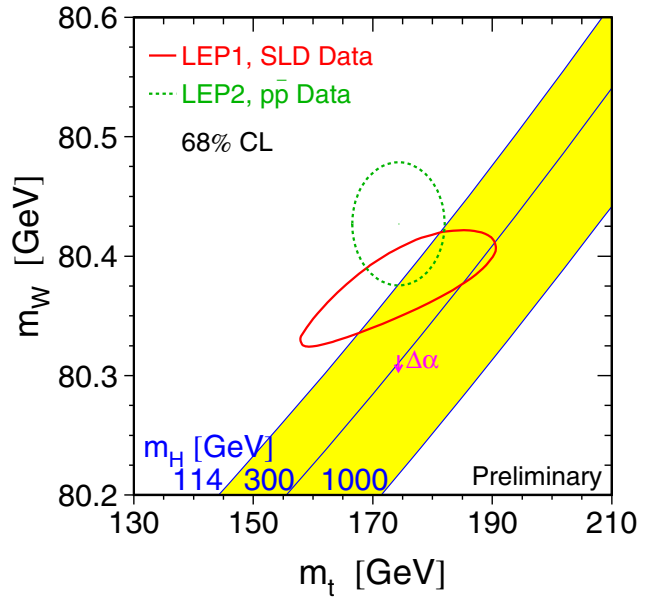

Fig. 39. Contours of W boson and top quark mass predicted by Z pole data, from direct measurement, and predicted by the SM as a function of Higgs boson mass

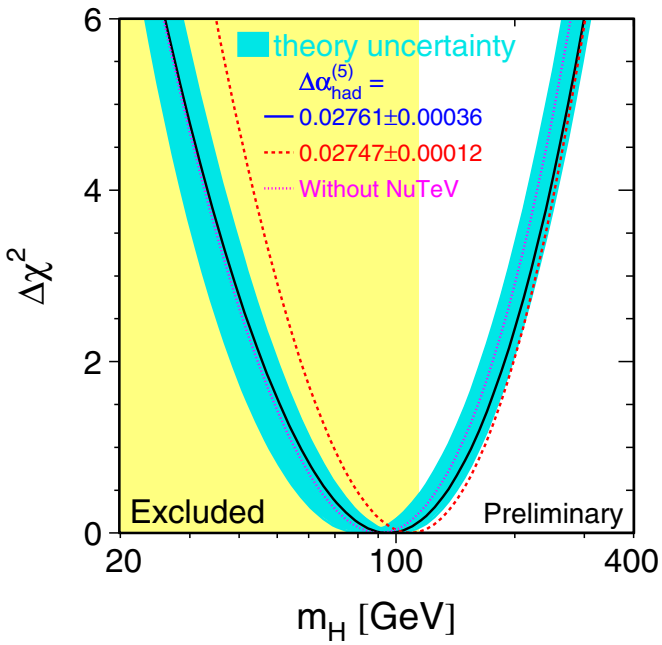

Fig. 40. The χ^2 as a function of Higgs mass from global fits to the full set of electroweak data. The *solid band* reflects the spread of theoretical uncertainties, and the region excluded by direct searches for the Higgs Boson is indicated

Table 7. Estimates of the precision of future experiments.

	M_W (MeV)	m_t (GeV)	$\sin^2\theta^{lept}_{eff}$
Now	34	5.1	0.00016
TeV IIB	17	1.3	0.00016
LHC	10	1.0	0.00016
LC	7	0.2	0.000085

shift in M_{Higgs}. The most likely value changes from 96 to 126 GeV, and the upper limit increases to 283 GeV.

Future experiments should dramatically reduce the uncertainties on electroweak parameters. Estimates for the Tevatron Run IIB, the LHC and a future Linear Collider (LC) are shown in Table 7 [34,35], taking the error on $\Delta\alpha^{(5)}_{had}(M_Z^2)$ to be 0.00012 in each case. The triple gauge couplings will also be measured with far greater precision. The impact of these future measurements on the prediction of the Higgs boson mass is illustrated in Fig. 41.

10 Conclusions

The electroweak Standard Model is tremendously successful in describing a range of parameters. Radiative corrections at loop level have been firmly established. However, there is no clear indication of the physics that is hoped to lie beyond. The largest discrepancies are only at the three standard deviation level. There is no experimental progress to be expected in the near future to resolve the difference in $\sin^2\theta^{lept}_{eff}$ derived from $A^{0,b}_{FB}$ and A_{LR}. The result from NuTeV has little impact on the global fit, but remains an unexplained deviation or fluctuation. The discrepancy between the measured and predicted values of the muon $(g-2)$ value has been reduced to about 2.5 standard deviations with the latest CMD-2 update. It is crucial to settle the inputs from such lower energy e^+e^- colliders, including radiative return results, before drawing conclusions there.

In the near future, the W mass measurement from LEP2 will be finalised, and new measurements of the W boson and top quark masses will be made using Tevatron Run II data. On a more practical note, the work of synthesising electroweak results and performing global electroweak fits will move across the Atlantic from the LEP Electroweak Working Group [26] to the Tevatron Electroweak Working Group [9]. In the longer term we may

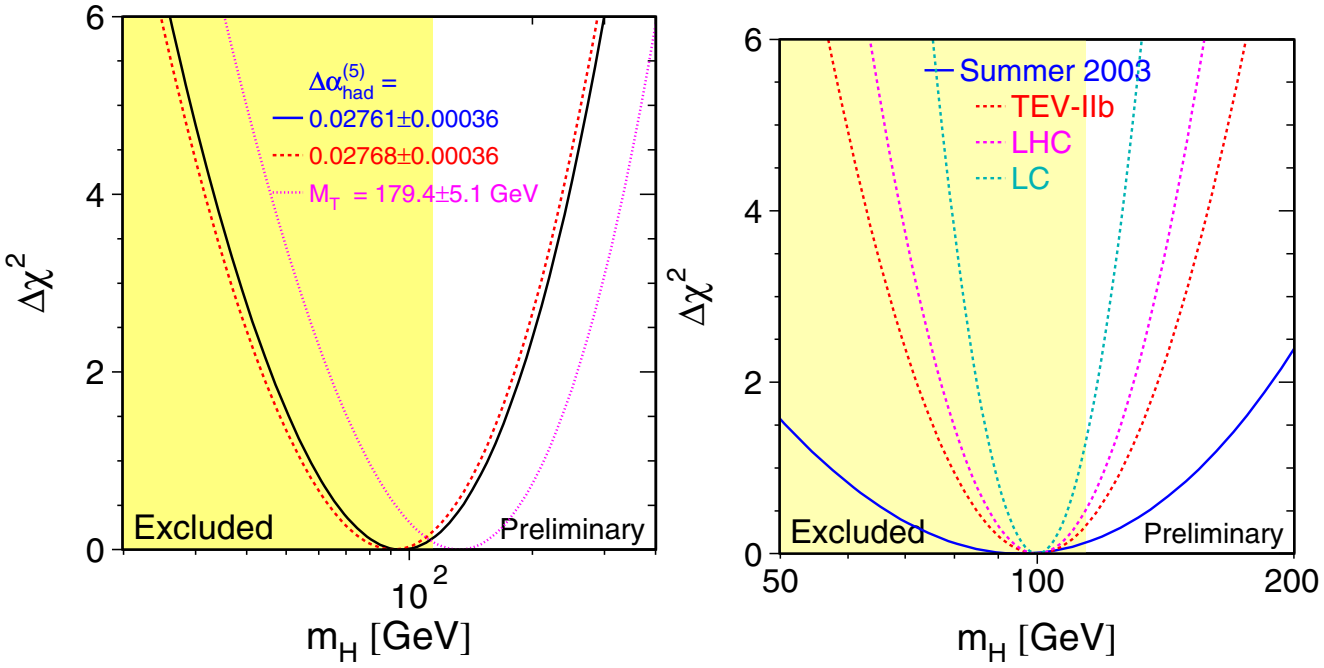

Fig. 41. The impact of using a shifted *top* quark mass or the latest value of $\Delta\alpha^{(5)}_{\rm had}(M_{\rm Z}^2)$ (*right*) and the impact of hypothetical future measurements (*right*) on the global electroweak fits

look forward to a direct measurement of the Higgs boson mass and maybe the discovery of a more complicated Higgs structure and other new particles. Most bewildering of all would be the absence of a detectable Higgs boson and no evidence of an alternative mechanism to replace it.

The full set of electroweak measurements places very strong constraints on any new physics. There are great prospects for further enlightenment in the near and not so near future.

Acknowledgements. It is a pleasure to thank the organisers for a stimulating conference in Aachen, and the many groups and individuals who provided results or helped with this review: LEP, SLD, CDF and D0 electroweak and top working groups, and in particular: P Azzi, E Barberis, E Barberio J Butterworth, D Charlton, R Chierici, B Clare, M Davier, S Eidelman, M Elsing, J Estrada, C Gerber, M Grünewald, A Heinson, A Kotwal, J Kühn, K McFarland, P Murat, P Newman, U Parzefall, B Pietrzyk, G Quast, C Rembser, M Schmitt, A Tapper, R Tenchini, T Teubner, M Verzocchi, T Wengler.

References

1. For a summary, see: The LEP Collaborations, ALEPH, DELPHI, L3, OPAL, the LEP Electroweak Working Group and the SLD Heavy Flavour Group, CERN-EP/2002-091
2. T. Kraemer: these proceedings
3. G. Anagnostou: these proceedings
4. `http://www.fnal.gov/pub/now/upgradeplan/`
5. A. Sidoti: these proceedings
6. N. Varelas: these proceedings
7. S. Natale: these proceedings
8. M. Bonesini: these proceedings
9. `http://tevewwg.fnal.gov`
10. W.L. Van Neerven and E.B. Zijlstra: Nucl. Phys. B **282**, 11 (1992)
11. R. Ofierzynski: these proceedings
12. R. Brunelière: these proceedings
13. M. Thomson: these proceedings
14. J. D'Hondt: these proceedings
15. P. de Jong: these proceedings
16. K.-P.O. Diener: these proceedings
17. E. Shabalina and W. Wagner: these proceedings
18. M. Warsinsky: these proceedings
19. B. Abbott et al.: D-Zero, Phys. Rev. D **58**, 052001 (1998)
20. T. Maruyama: these proceedings
21. Muon $(g-2)$ and G.W. Bennett et al.: Phys. Rev. Lett. **89**, 101804 (2002); Erratum-ibid. **89**, 129903 (2002)
22. T. Teubner: these proceedings
23. M. Davier, S. Eidelman, A. Höcker, and Z. Zhang: hep-ph/0208177.v3
24. K. Hagiwara, A.D. Martin, D. Nomura, and T. Teubner: hep-ph/0209187
25. M. Incagli and J. Kühn: these proceedings
26. `http://lepewwg.web.cern.ch/LEPEWWG/`
27. H. Burkhardt and B. Pietrzyk: Phys. Lett. B **513**, 46 (2001)
28. J.F. de Troconiz and F.J. Yndurain: Phys. Rev. D **65**, 093002 (2002)
29. R.R. Akhmetshin et al.: CMD-2, hep-ex/9904027
30. R.R. Akhmetshin et al.: CMD-2, Phys. Lett. B **527**, 161 (2002)
31. B. Pietrzyk and H. Burkhardt: LAPP-EXP/2003-07
32. G. Quast: these proceedings
33. M.Y. Kuchiev and V.V. Flambaum: hep-ph/0305053
34. U. Baur et al.: Snowmass 2001, hep-ph/0111314
35. TESLA TDR, Part III, Editors: R.D. Heuer, D. Miller, F. Richard, and P. Zerwas: DESY 2001-011